Central European Geology, Vol. 62/1, 1–14 (2019)
DOI: 10.1556/24.61.2018.09
First published online July 16, 2018

Image processing for fractal geometry-based discrete fracture network modeling input data: A methodological approach

Dorottya Kovács[1]*, Gergely Dabi[2], Balázs Vásárhelyi[1]

[1]Faculty of Civil Engineering, Department of Engineering Geology and Geotechnics, Budapest University of Technology and Economics, Budapest, Hungary
[2]Faculty of Science and Informatics, Department of Mineralogy, Geochemistry and Petrology, University of Szeged, Szeged, Hungary

Received: July 29, 2017; accepted: March 4, 2018

With the intent of making data acquisition for fractal geometry-based discrete fracture network (DFN) modeling time-efficient and automatized, a new method was established. For the automation of data retrieval from the images of the studied surfaces, a series of image-processing operations and MATLAB algorithms have been developed. The method allows the retrieval of more than 1,000 fracture-length data/cm^2 of one sample in several minutes. This methodology tends to be a useful tool in studies of fracture network geometries. DFN models of a supposed excavated and/or environmental damage zone, designed with the use of data supplied by the above method, are presented in this work as an example.

Keywords: image processing, fracture network, fractal geometry, MATLAB, EDZ

Introduction

Investigation of the spatial distributions of microfracture networks in fractured rock bodies is essential for the accurate understanding of the mechanical behavior and fluid flow within the rock mass when designing underground facilities. Rock mechanics

*Corresponding author: Dorottya Kovács; Faculty of Civil Engineering, Department of Engineering Geology and Geotechnics, Budapest University of Technology and Economics, P.O.B. 91, H-1521 Budapest, Hungary
E-mail: kovacs.dorottya@epito.bme.hu

ISSN 1788-2281

suggests that most mechanical parameters are related to the inherent microcrack system of the rock (Kemeny and Cook 1991).

Retrieval of relevant data for the characterization of fracture geometry is a tedious and time-consuming task, but it is essential in discrete fracture network (DFN) modeling. DFN modeling is a widely used tool in rock mechanics (Jing 2003) and hydrogeologic practice (Long 1996); thus, underground designing and reservoir modeling-related research may benefit from it as well. In this study, a fractal geometry-based DFN model was developed, which requires the following input data (Tóth and Vass 2011):

- fractal dimension for fracture centers,
- parameters (E and F) of the fracture length distribution,
- lower and upper extreme fracture length values,
- aperture, which must be given as a function of length with two input parameters (Vermilye and Scholz 1995), because it is not treated as an independent variable, and
- dip direction and dip angle data can be given as an explicit set of data pairs instead of a distribution function.

For the automatization of data retrieval, a sequence of image-processing operations and algorithms was developed (Fig. 1), which is introduced in this paper.

Materials and methods

Sample preparation and image creation

Specimens used in this study were drilled from the floor of an investigation tunnel, which was constructed using the Drill and Blast technique (Langefors and Khilstrom 1973). The specimens were prepared as cylinders of 68 mm diameter and 50 mm length. The material used in this study was coarse-grained leucocratic granite (LGr, seven specimens) and banded gneiss (BGn, nine specimens).

From the granite and gneiss specimens, 5-mm-thick disks were cut from the cylinders and their surfaces were polished after impregnation with UV fluorescent-tinted epoxy. This made the direct observation of the crack geometries possible in refracted UV illumination (Fig. 2a). Images of the discs were taken with an Olympus DP73 camera mounted on an Olympus BX41 microscope with 1.25× magnification. The microscope was used in reflected light mode with a 100-W U-LH100HG mercury vapor lamp as light source and an Olympus U-MWBV2 filter cube installed (excitation range between 400 and 440 nm).

Image processing

The same image-processing method was applied for all images of the two rock types. The first step of the image processing is the segmentation of the UV

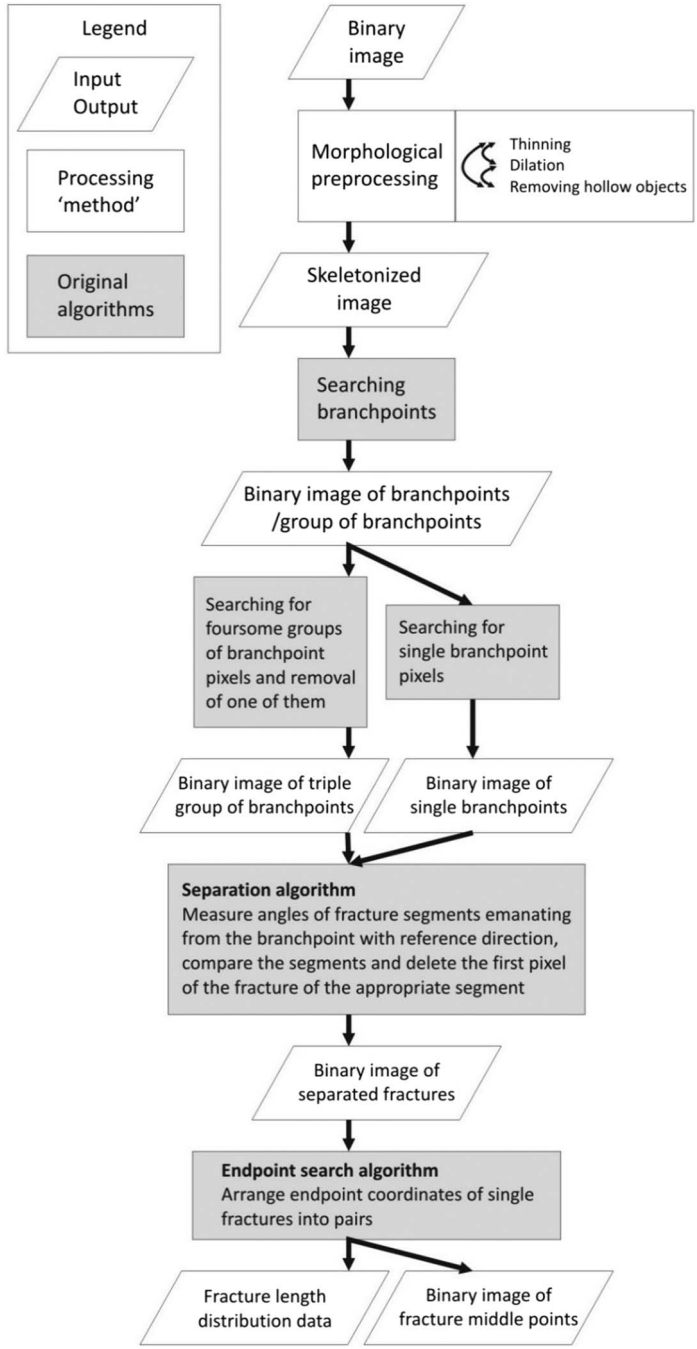

Fig. 1
Steps of the image processing including the algorithms

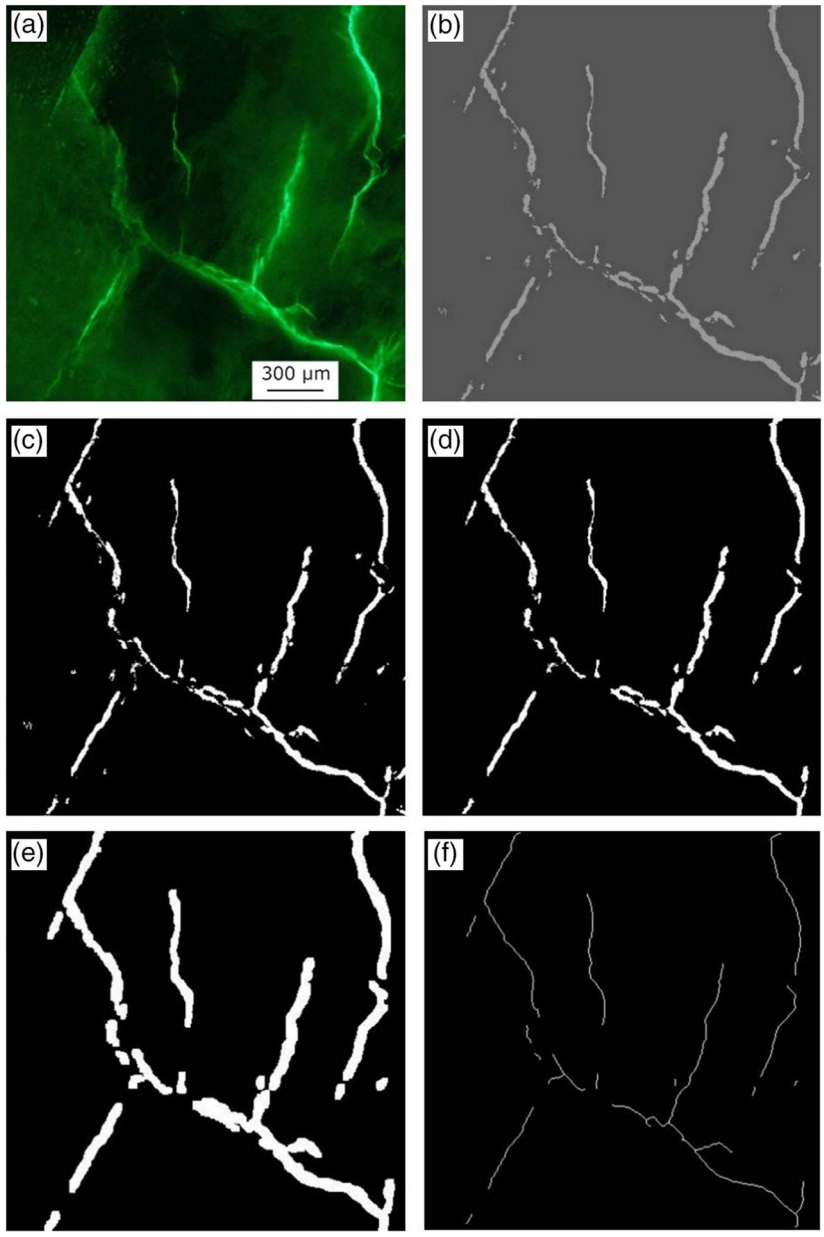

Fig. 2
The performed image-processing steps detailed in the text. (a) Crack geometry in refracted UV illumination. (b) Gray scale image. (c) Binary image. (d) Image after filtration. (e) Crack geometry after dilatation. (f) Skeletonized image of the fracture network

fluorescence images, i.e., the division of the pixels of the images into microcracks and host rock. To achieve this, the original RGB images were processed by Trainable Weka Segmentation plugin, which is available in the ImageJ-based Fiji environment (Schindelin et al. 2012). The Trainable Weka Segmentation plugin enables the user to train the software to distinguish and classify segments of the image by drawing lines and marking out areas, thereby collecting information on pixels' gray level and their spatial variation.

The following image-processing steps, including the algorithms, are shown in a flowchart in Fig. 1. The segmentation step results in 8-bit gray scale images (Fig. 2b). It is unavoidable to end up with misidentified image segments following the segmentation treatment. These objects are mainly fluorescent mineral grains of nearly isometric shape. Due to the obvious difference of the shape of fractures and that of the nonlinear objects, these groups of pixels can be easily filtered out with the use of the appropriate built-in image-processing procedures in MATLAB (e.g., Arena et al. 2014).

First, the 8-bit gray scale image (Fig. 2b) is converted into a binary black-and-white image (Fig. 2c). In the black-and-white image, white pixels represent microfractures and voids and black pixels represent the intact host rock. Next, noise and small objects (generally fluorescent mineral grains) are filtered from the data by selecting the retaining 1,000 largest objects (i.e., largest groups of associated white pixels) on the image, which effectively removes isolated pixels or small pixel groups (Fig. 2d). The morphological processing begins with dilatation (Pratt 2001; Fig. 2e), which thickens the objects and removes interior irregularities (i.e., holes inside pixel groups representing microfractures) and those along their boundaries (i.e., embayments).

Originally, continuous cracks can appear as a sequence of individual parallel microfractures in line, which can reunite during dilatation. However, originally distinct microcracks can also coagulate during dilatation; these are separated in the next step, based on their relative angles to the reference direction of the image (see later). Dilatation is necessary because internal irregularities in the image yield additional spurious microcracks during thinning in the final step of the process; it should be repeated as many times as needed. This should be carefully controlled by the user and maintained close to the original image.

After achieving the ideal connectivity of the objects (as defined by the user by checking the image between subsequent dilatation steps), filtering is carried out based on the objects' Euler number (see MATLAB's Image Processing Toolbox for details). The Euler number specifies the number of objects in a region minus the number of holes in those pixel groups. This step extracts circular elements, which are generally inherited from planar objects, such as UV fluorescent minerals. Removing elements with negative Euler numbers, i.e., eliminating objects that have internal holes, like braided crack systems, from the image can also be done, but this step needs to be carried out carefully. Finally, the remaining objects should be thinned until they are 1-pixel wide (Pratt 2001). This process results in a skeletonized image of the fracture network (Fig. 2f).

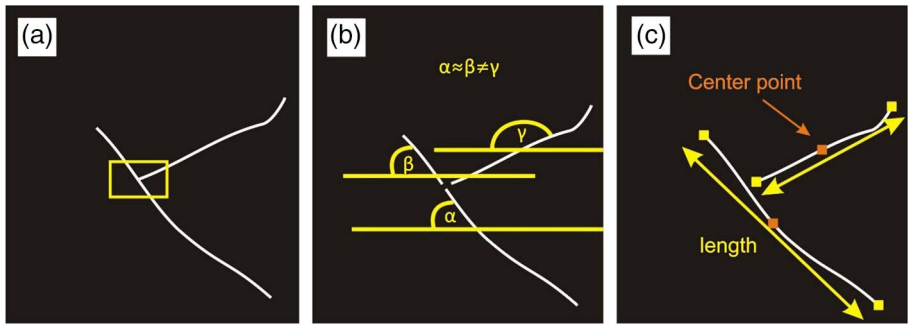

Fig. 3
Schematic image of the data retrieval algorithm. (a) Branchpoint searching. (b) Division of branching microcracks based on their relative trends. (c) Length measurement and center point coordinate calculation

Data retrieval

Since the algorithm prints out the connected pixels of individual fractures, branching microcracks need to be dismembered at branchpoints. To do this, a MATLAB algorithm was developed. The code can be obtained from the primary author of this paper. The algorithm first finds the branchpoints (Fig. 3a); then it calculates the angle between the cracks emanating from the branchpoint and a reference line (the horizontal line of the studied image; Fig. 3b). It is assumed that the fractures with similar angles are part of the same crack and the pixel that connects the third fracture to the branchpoint is removed. By defining the branchpoint pixels to remove, branching microcracks are divided into multiple cracks, increasing the total number of single fractures. As the final step of the image processing, another MATLAB algorithm pairs with fracture endpoints, which are printed out as an array of coherent end-point coordinates. This array is then used to calculate microcrack lengths and center coordinates (Fig. 3c).

The fractal dimension values of both the entire fracture network and the centers of the single cracks were defined using the Box counting method (Barton 1995; Mandelbrot 1983) using the Benoit 1.3 software. The input images for the fractal analysis were the binary segmented images and the images showing the center coordinates of each fracture, which were processed in MATLAB.

Case study

Fracture network modeling

Based on the fracture length distribution, the fractal dimension of the fracture centers, and the orientation and aperture of the fractures, simulations of the 3D microcrack system were fulfilled using a fractal geometry-based DFN code (RepSim). Details of the algorithms used in RepSim are discussed by Tóth et al. (2004), Tóth (2010), Tóth and Vass (2011), Bauer and Tóth (2016), and Tóth (2018). RepSim is stochastic in the sense

that it obtains a certain number of equally probable realizations. The final output form of the fracture network corresponds to the initial expectations, where the parameters of this network are equal to the parameter distribution of the originally studied fracture network.

Dip direction and dip angle data were imported into the model from a given data set based on macroscale fractures. Aperture of the fractures was given as a function of length.

The RepSim fracture network models were built to represent 10 m^3 volumes with different proportions of the studied rock types (Fig. 4), the constituent cells of which

	Number of clusters, that are larger than 50 pieces	Number of fractures in the largest cluster
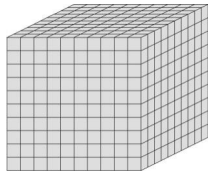	9	84
	14	100
	17	101
	7	109
	10	74
	Number of clusters, that are larger than 100 pieces	Number of fractures in the largest cluster
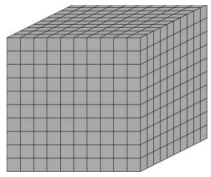	47	498
	52	583
	47	310
	52	256
	43	393
	Number of clusters, that are larger than 100 pieces	Number of fractures in the largest cluster
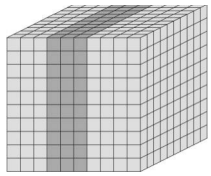	16	208
	12	150
	13	220
	18	225
	11	203
	Number of clusters, that are larger than 100 pieces	Number of fractures in the largest cluster
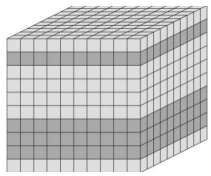	15	252
	15	179
	14	204
	20	193
	19	217
	Number of clusters, that are larger than 100 pieces	Number of fractures in the largest cluster
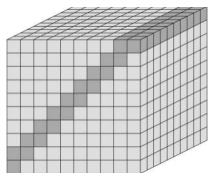	11	215
	11	194
	11	201
	7	213
	10	237

Fig. 4
Summary of the built models with their five realizations. The light gray color represents the leucocratic granite and the dark gray represents the banded gneiss in the modeled volume

are 1 m^3 cubes. For the length distribution function, an interval of the fracture lengths of interest needs to be given by the user, which was between 50 and 1,500 mm in this study. Each configuration was run for five times; thus, five equally probable realizations were generated based on the measured parameters.

Results

The defined fractal dimension values of the fracture network in the gneiss scatter between 1.59 and 1.78 and in the granite between 1.61 and 1.69 (Fig. 5). The smaller range in fractal dimension values in granite compared with gneiss is worth mentioning. Neither fractal dimensions of the fractures in the gneiss nor those in the granite show any definite trend with increasing distance from the tunnel surface.

From the length data set of each specimen, length distribution histograms (Fig. 6) were generated. For the determination of the distribution function, it is crucial to find the appropriate bin widths of the fracture length histogram. If the bin width is too low, the number of fractures is not sufficient, whereas by choosing a wide bin, the number of fractures in an interval is too high, both of which influence the slope of the log transform. To define the proper width of the intervals (k), the commonly used rule was applied:

$$k = 2 \times \mathrm{INT}(\log_2(\max(L))),$$

where INT is the integer function, L is the length, and in this case k was 12.

After log–log transformation (Fig. 7) of the data, the fitted linear regression line defines the parameters of the distribution function. E is the slope of the regression line and F is where it crosses the y axis.

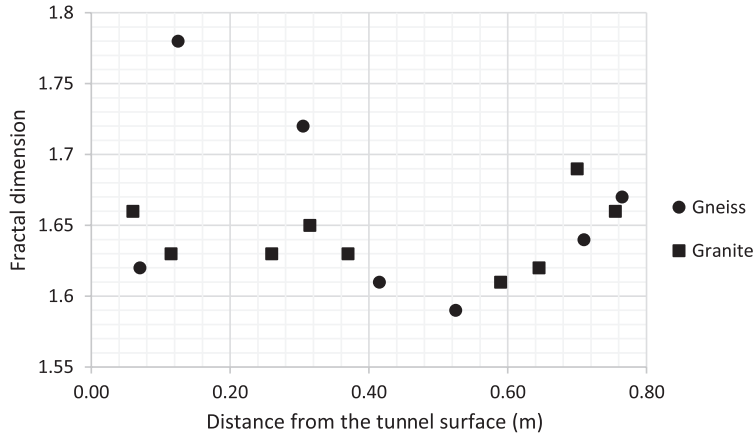

Fig. 5
Fractal dimension values varying with the distance from the tunnel surface

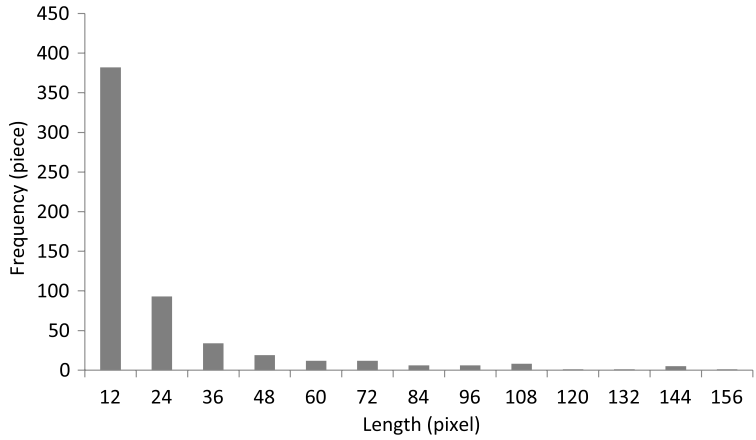

Fig. 6
Length distribution histogram of a granite specimen

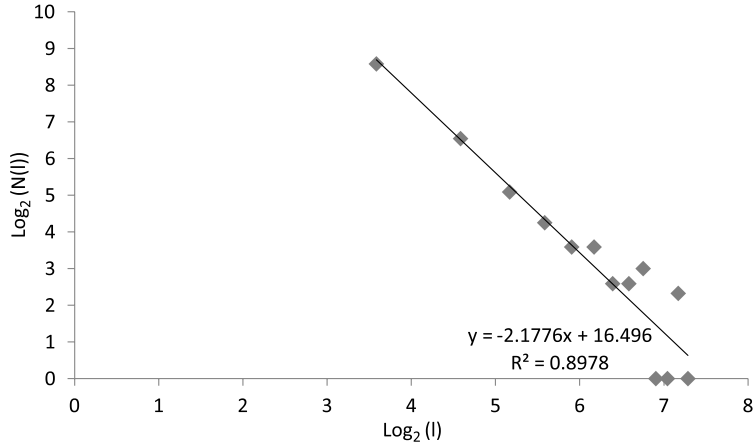

Fig. 7
Log–log transformation of the length distribution of a granite specimen

After removing the outlying data points, the parameters E and F can be taken from the equation of the line (Fig. 8). Table 1 summarizes the resulted E and F values of the studied specimens.

In the case where the entire 10 m^3 rock volume was composed of gneiss (BGn), simulations yielded ~181,000 fractures in the model. According to these simulations, the highest number of communicating fracture subclusters was ~20, while the largest cluster consisted only of about 100 communicating fractures. Five simulations of the model with the entire rock volume built of granite (LGr) show that the highest number

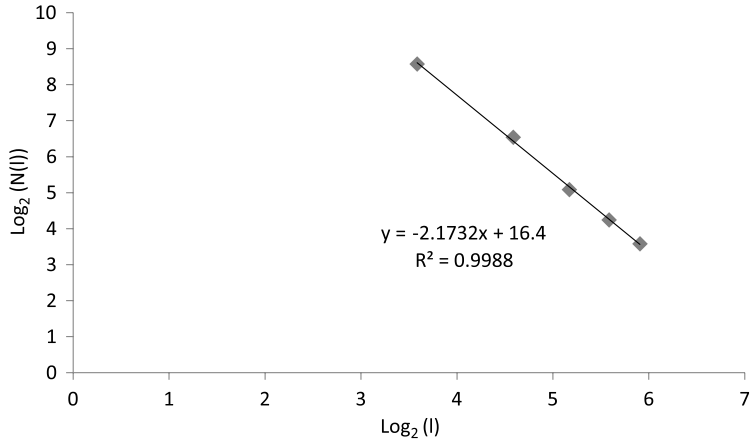

Fig. 8
The fitted regression line, which gives the parameters of the distribution functions of a granite specimen. In this case, $E = -2.17$ and $F = 16.4$

of communicating fracture clusters was 52, while the largest number of communicating fractures in one cluster was about 600 out of 231,000 fractures. In the granite case, the fractures are oriented in two preferred orientations, and relatively longer fractures are found when comparing with those typical in the gneiss. The models that consisted of both rock types vary between the values characteristic for the studied gneiss and granite, depending on the amount of each component (Fig. 4). According to the simulated fracture network models, the largest percolation cluster sizes are between 0.06% (gneiss) and 0.25% (granite) of all fracture systems.

Discussion and conclusions

If one requires the characterization of every single element of the population, then the analysis of linear-shaped objects such as fractures is complicated. To define the spatial interactions and separation processing of an interconnected network visualized on images, the most commonly applied method is overdrawing the linear objects freehanded in appropriate software such as ArcGIS or CorelDraw (Tóth and Kamera 2010). This technique may be burdened with uncertainty caused by human factors and it can be also very time consuming if applied to large number of images.

There are several automated methodologies focused on the detection of macroscopic surface cracks in concrete, which are visualized using a digital camera (Chen and Hutchinson 2010; Dare et al. 2002; Jahanshahi and Masri 2013; Lee et al. 2013; Zhu et al. 2011). However, all these were specifically developed for field applications and limited to a few non-interacting cracks per field of view. In the case of microcracks

Table 1
Parameters of the distribution function

Specimen	*E*	*F*
	2.24	18.18
	2.23	18.54
	1.85	16.77
Gneiss	2.07	16.95
	2.82	21.06
	2.51	20.00
	1.90	15.90
Average	2.23	18.20
Variance	0.12	3.41
	2.17	16.40
	1.92	15.47
	1.93	15.91
	2.35	18.24
Granite	1.65	14.69
	2.24	17.68
	2.25	17.81
	1.96	16.80
	1.99	16.80
Average	2.05	16.64
Variance	0.05	1.35

in crystalline rocks, a far larger population of linear objects and their statistical analysis is needed; due to the complexity of the interconnected networks, the problem of fracture separation arises. Following the approaches of Arena et al. (2014), Ito et al. (2002), and Le Roux et al. (2013), a joint methodology of image processing and data retrieval, with an initial stage of material preparation, was developed.

As the introduced coupled method starts with sample preparation, it definitely limits its adaptability to rocks that can be ground and impregnated. It is unavoidable to impregnate all the voids with the tinted epoxy; therefore, in the case of rock with porosity that is related not only to fracturing but has also, for instance, to internal caverns or pores, the technique is not applicable. The filtering of isolated pixel groups based on their size

could be considered as a possible issue in terms of losing fractures from the statistical analysis with a very small size range. However, the scale issue is a universal problem for all methods; the size range of the fractures desired to be examined must be set in all cases with prudence. Sometimes, this may require necessary abandonment of data.

The data acquisition method developed for the retrieval of the relevant geometric parameters of fracture systems was a convenient tool to determine the variables required for DFN modeling, as shown in this study. The studied specimens showed a very small number of interconnected fractures and the hydrological communication between fractures is constantly negligible. However, the ability to discriminate between two rock types of very small crack density indicates the usefulness of the developed method. There is no detectable trace of an excavated and/or environmental damage zone, as the fractal dimension of the fractures does not show a definite trend with distance from the tunnel surface.

The presented method provides the opportunity to gain information about the spatial and length distribution of microfracture networks form hand specimens (Figs 9 and 10). The automatization of the data retrieval resulted in a user-friendly and time-effective solution that is less susceptible to human factors.

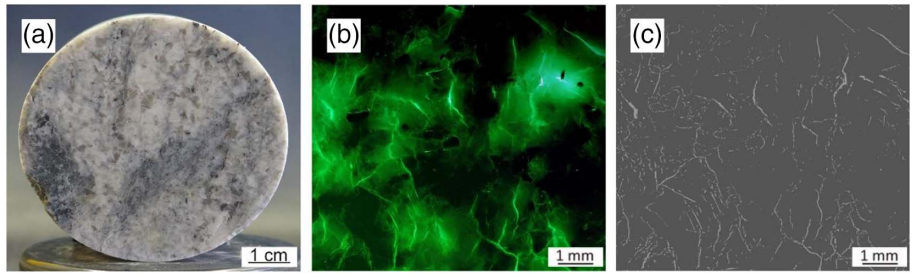

Fig. 9
Images of a granite specimen. (a) Core sample. (b) UV illuminated image after fluorescent impregnation. (c) Segmented image

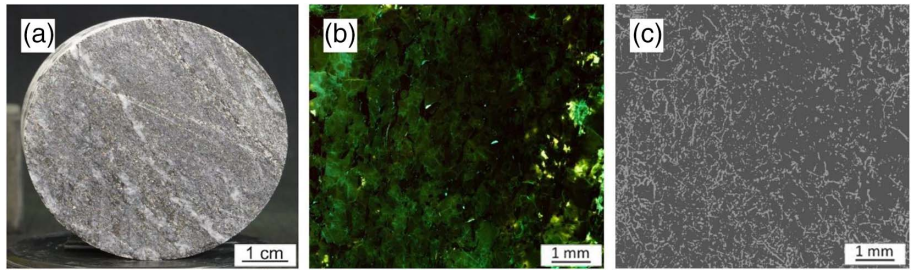

Fig. 10
Images of a gneiss specimen. (a) Core sample. (b) UV illuminated image after fluorescent impregnation. (c) Segmented image

References

Arena, A., C. Delle Piane, J. Sarout 2014: A new computational approach to cracks quantification from 2D image analysis: Application to micro-cracks description in rocks. – Computers & Geosciences, 66, pp. 106–120.

Barton, C.C. 1995: Fractal analysis of scaling and spatial clustering of fractures. – In: Barton, C.C., P.R. La Pointe (Eds): Fractals in the Earth Sciences. Plenum Press, New York, 168 p.

Bauer, M., T.M. Tóth 2016: Characterization and DFN modelling of the fracture network in a Mesozoic karst reservoir: Gomba oilfield, Paleogene Basin, Central Hungary. – Journal of Petroleum Geology, 40/3, pp. 319–334.

Chen, Z., T.C. Hutchinson 2010: Image-based framework for concrete surface crack monitoring and quantification. – Advances in Civil Engineering, 2010, pp. 1–18.

Dare, P., H. Hanley, C. Fraser, B. Riedel, W. Niemeier 2002: An operational application of automatic feature extraction: The measurement of cracks in concrete structures. – Photogrammetry and Remote Sensing, 17/99, pp. 453–464.

Ito, A., Y. Aoki, S. Hashimoto 2002: Accurate extraction and measurement of fine cracks from concrete block surface image. – In: Proceedings of the IEEE 28th Annual Conference of the Industrial Electronics Society, IECON 02, 3, pp. 2202–2207.

Jahanshahi, M.R., S.F. Masri 2013: A new methodology for non-contact accurate crack width measurement through photogrammetry for automated structural safety evaluation. – Smart Materials and Structures, 22/3, p. 035019.

Jing, L. 2003: A review of techniques, advances and outstanding issues in numerical modelling for rock mechanics and rock engineering. – International Journal of Rock Mechanics & Mining Sciences, 40, pp. 283–353.

Kemeny, J.M., N.G.W. Cook 1991: Micromechanics of deformation in rocks. – In: Shah, S.P. (Ed): Toughening Mechanisms in Quasi-Brittle Materials. Nato Science Series E. Springer, 195, pp. 155–188.

Langefors, U., B. Khilstrom 1973: The Modern Technique of Rock Blasting (2nd ed.) – Wiley, New York, 405 p.

Le Roux, S., F. Medjedoub, G. Dour, F. Rézaï-Aria 2013: Image analysis of microscopic crack patterns applied to thermal fatigue heat-checking of high temperature tool steels. – Micron, 44, pp. 347–358.

Lee, B.Y., Y.Y. Kim, S.-T. Yi, J.-K. Kim 2013: Automated image processing technique for detecting and analyzing concrete surface cracks. – Structure and Infrastructure Engineering, 9/6, pp. 567–577.

Long, J.C.S. (Ed) 1996: Rock Fractures and Fluid Flow: Contemporary Understanding and Applications. – National Academy Press, 551 p.

Mandelbrot, B.B. 1983: The Fractal Geometry of Nature. – Freeman, 468 p.

Pratt, W.K. 2001: Digital Image Processing PIKS Inside. – Wiley, 762 p.

Schindelin, J., I. Arganda-Carreras, E. Frise, V. Kaynig, M. Longair, T. Pietzsch, S. Preibisch, C. Rueden, S. Saalfeld, B. Schmid, J.-Y. Tinevez, D.J. White, V. Hartenstein, K. Eliceiri, P. Tomancak, A. Cardona 2012: Fiji: An open-source platform for biological-image analysis. – Nature Methods, 9, pp. 676–682.

Tóth, T.M. 2010: Determination of geometric parameters of fracture networks using 1D data. – Journal of Structural Geology, 32, pp. 878–885.

Tóth, T.M. 2018: Fracture network characterization using 1D and 2D data of the Mórágy Granite body, southern Hungary. – Journal of Structural Geology, 113, pp. 176–187.

Tóth, T.M., R. Kamera 2010: Repedésrendszer legfontosabb tulajdonságainak elemzésére és a vizsgált paraméterek térbeli kiterjesztésére alkalmazható elemzési eljárás módszertani kidolgozása, ellenőrzése és optimalizálása [Methodological developement, verification and optimization for analysis of the most important fracture system properties and the spatial extension of the examined parameters]. – Manuscript, RHK Kht., Paks, 106 p. (in Hungarian).

Tóth, T.M., É. Szűcs, F. Schubert, Cs. Hollós 2004: Conceptual fracture network model of the crystalline basement of the Szeghalom Dome (Pannonian Basin, SE Hungary). – Acta Geologica Hungarica, 47/1, pp. 19–34.

Tóth, T.M., I. Vass 2011: Relationship between the geometric parameters of rock fractures, the size of percolation clusters and REV. – Mathematical Geosciences, 43, pp. 75–97.

Vermilye, J.M., C.H. Scholz 1995: Relation between vein length and aperture. – Journal of Structural Geology, 17, pp. 423–434.

Zhu, Z., S. German, I. Brilakis 2011: Visual retrieval of concrete crack properties for automated post-earthquake structural safety evaluation. – Automation in Construction, 20/7, pp. 874–883.